Goos-Hänchen shifts of the reflected waves from a cold, inhomogeneous, and magnetized plasma slab

Guoding Xu,* Taocheng Zang, and Tao Pan
Department of Physics, Suzhou University of Science and Technology, Suzhou 215009, People's Republic of China
(Received 7 October 2009; published 7 January 2010)

We discuss theoretically the Goos-Hänchen (GH) shifts of the reflected waves from a cold, inhomogeneous, and magnetized plasma slab by using the invariant imbedding approach. Aiming at the linear and parabolic electron-density profiles, we demonstrate numerically the dependences of the co- and cross-polarized GH shifts on the angle of incidence, external static magnetic field, and the thickness of the plasma slab. The results show that the different electron-density profiles of plasma can result in the very different dependences of the GH shifts on the angle of incidence, external magnetic field, and the slab's thickness; the GH shifts can be switched between the considerably large positive and negative values under certain conditions. Particularly, without altering the structure of the plasma slab, the GH shifts can be manipulated by modifying the angle of incident or the external static magnetic field.

DOI: 10.1103/PhysRevE.81.016603 PACS number(s): 41.20.Jb, 42.25.Dd, 52.35.Hr, 78.20.Bh

I. INTRODUCTION

As has been known, the reflected beam can experience a lateral shift with respect to the path predicted by geometrical optics when a total internal reflection happens at the interface separating two media. This lateral shift is the so-called Goos-Hänchen (GH) shift. Since it was discovered by Goos and Hänchen [1,2] and explained theoretically by Artmann [3] in the late 1940s, the GH shift has long been a subject of extensive research in various fields such as micro- and nano-optics [4], acoustics, quantum mechanics, and plasma physics . In practice, the GH shift effect is not confined to the total internal reflection situation; during partial reflection, this effect can also show up, especially in the slab configurations, where both the reflected and transmitted beams might undergo a lateral shift. In this regard, much work has been conducted in different circumstances, such as transparent dielectric slabs [5–11], negatively refractive slab [12–14], indefinite medium slab [15], slab of electro-optic crystal [16], and gyrotropic slab [17].

Theoretically, the GH shift is usually studied on the basis of the stationary-phase approach, which is mainly revealed by the Artmann's formula [3,5–19], i.e., $\Delta=-\partial\varphi/\partial k_x$, where φ is the phase shift of the reflected or transmitted beam with respect to the incident beam and k_x is the wave-vector component parallel to the interface. Clearly, the physical and structured parameters of the materials, such as the permittivity, permeability, and the periodicity and layer thicknesses of constituents, affect the phase shifts as well as the surface (or interface) properties and hence cause the changes of the GH shifts. In consequence, the GH shifts can be controlled by modulating the permittivity, permeability, and structures of the materials. Chen *et al.* [16] achieved the tunable GH shifts in electro-optic crystals by virtue of the applied electric field; Huang *et al.* [17] obtained the positive and negative GH shifts by adjusting the applied magnetic field; Wang *et al.* [18] controlled the GH shift via a coherent driving field. The GH shift effect in photonic crystals [19,20] and in the process of surface-polariton excitation [13,21,22] should originate from the changes of structures and surface (or interface) properties.

The GH shift effect in the homogeneous media has been explored extensively; however, so far the studies of the GH shift in inhomogeneous media have been still missing, which might be due to the great difficulties in theory. More recently, Kim *et al.* [23] presented a new version of the invariant imbedding theory for the propagation of coupled waves in arbitrarily inhomogeneous stratified media, and applied it successfully to the study of mode conversion in inhomogeneous plasmas [24,25]. The main idea of this theory is to transform the original boundary-value problem of wave equations, which are second-order differential equations, into an initial value problem of coupled first-order ordinary differential equations for the reflection and transmission coefficients and the electric and magnetic field amplitudes. Employing the theory, one can obtain exact solutions for the reflection and transmission coefficients and the field amplitudes inside arbitrarily inhomogeneous stratified media, including stratified nonlinear [26] and random [27] media. Based on this theory, in this paper, we discuss theoretically the GH shifts of the reflected waves from a cold, inhomogeneous, and magnetized plasma slab, where the inhomogeneity stems from the inhomogeneous electron density. Here, the inhomogeneity and the applied magnetic field are actually responsible for the tunings of the plasma's permittivity. Therefore, it is potentially possible to yield a number of new phenomena in such materials.

In Sec. II, we present the invariant imbedding equations for the reflection and transmission coefficients and the GH shifts determined by the stationary-phase approach. Aiming at two kinds of electron-density profiles, i.e., the linear and parabolic profiles, the dependences of the GH shifts of the co- and cross-polarized components in the reflected wave on the angle of incidence, applied magnetic field, and thickness of the plasma slab are illustrated in Sec. III. The main conclusions are summarized in Sec. IV.

*Corresponding author. FAX: +86-512-68418473; guodingxu@163.com

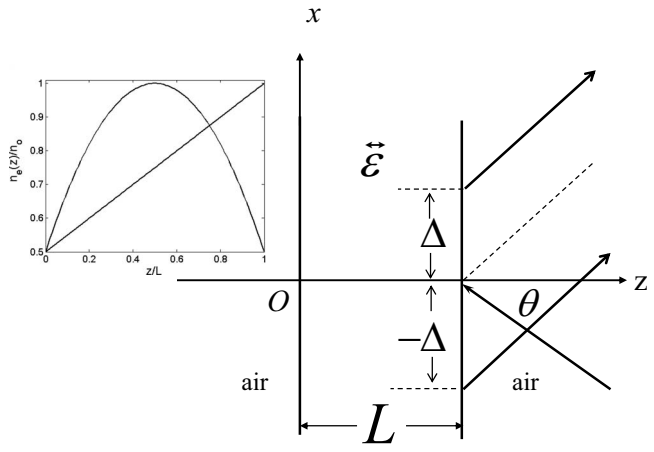

FIG. 1. Schematic of the cold, inhomogeneous, and magnetized plasma slab. External static magnetic field is directed along the x axis. Dashed line is the path of reflection usually expected from geometrical optics. Inset in the upper left shows the linear and parabolic electron-density profiles.

II. MODEL AND COMPUTATIONAL METHOD

Consider a cold, inhomogeneous, and magnetized plasma slab in air occupying the range $0 \le z \le L$, where both the electron density n_e and the dielectric permittivity $\vec{\vec{\varepsilon}}$ are only z dependent. Let an arbitrarily polarized plane monochromatic electromagnetic wave of angular frequency ω be incident at an angle θ on the interface $z=L$ from the right, as sketched in Fig. 1. For simplicity, we restrict our attention to the case where the external static magnetic field is applied perpendicularly to the direction of inhomogeneity, *viz.*, $\vec{B}_0 = B_0 \hat{x}$, with $\hat{x}$ being the unit vector along the x direction. For the above geometry, the permittivity tensor $\vec{\vec{\varepsilon}}$ of the cold plasma for high-frequency wave is written as

$$\vec{\vec{\varepsilon}} = \begin{pmatrix} \varepsilon_3 & 0 & 0 \\ 0 & \varepsilon_1 & -i\varepsilon_2 \\ 0 & i\varepsilon_2 & \varepsilon_1 \end{pmatrix}, \tag{1}$$

with

$$\varepsilon_1 = 1 - \frac{\omega_p^2(\omega + i\nu)}{\omega[(\omega + i\nu)^2 - \omega_c^2]}, \quad \varepsilon_2 = \frac{\omega_p^2 \omega_c}{\omega[(\omega + i\nu)^2 - \omega_c^2]}, \tag{2}$$

$$\varepsilon_3 = 1 - \frac{\omega_p^2}{\omega(\omega + i\nu)},$$

where the constant ν is the phenomenological collision frequency; $\omega_c = eB_0/2m$ is the electron cyclotron frequency and e and m are the electron's charge and mass, respectively. For the inhomogeneous electron density, it will be convenient to express the plasma frequency ω_p as

$$\omega_p^2 = \frac{e^2}{m\varepsilon_0} n_e(z) = \omega_0^2 f(z), \tag{3}$$

where $\omega_0 = \sqrt{n_0 e^2/m\varepsilon_0}$ is the local plasma frequency, n_0 is the local electron density, and $f(z)$, a dimensionless function of z, describes the electron-density profiles. So, Eq. (2) can be rewritten in the z-dependent form

$$\varepsilon_1 = 1 - \frac{\omega_0^2(\omega + i\nu) f(z)}{\omega[(\omega + i\nu)^2 - \omega_c^2]}, \quad \varepsilon_2 = \frac{\omega_0^2 \omega_c f(z)}{\omega[(\omega + i\nu)^2 - \omega_c^2]}, \tag{4}$$

$$\varepsilon_3 = 1 - \frac{\omega_0^2 f(z)}{\omega(\omega + i\nu)}.$$

Evidently, ε_1, ε_2, and ε_3 are all the functions of the spatial coordinate z.

As known, there exist two eigenmodes in the magnetized plasma, called the ordinary (O) and extraordinary (X) modes, respectively, but the O and X modes are no longer the eigenmodes and couple to each other if the plasma is inhomogeneous. Anyway, the electric and magnetic fields of waves in the plasma slab must satisfy the following equations, as derived from Maxwell's equations:

$$\vec{\nabla} \times (\vec{\nabla} \times \vec{E}) = k_0^2 \vec{\vec{\varepsilon}} \cdot \vec{E}, \tag{5a}$$

$$\vec{\nabla} \times (\vec{\vec{\varepsilon}}^{-1} \vec{\nabla} \times \eta_0 \vec{H}) = k_0^2 \eta_0 \vec{H}, \tag{5b}$$

where $k_0 = \omega/c$ and $\eta_0 = \sqrt{\mu_0/\varepsilon_0}$ are the wave vector and wave impedance in vacuum, respectively, and c is the speed of light in vacuum. For an arbitrarily polarized plane wave propagating within the xz plane, we assume that all field components without the y dependence depend on x and t through a factor $e^{i(qx-\omega t)}$, where $q = k_0 \sin\theta$ is the x component of the wave vector. Eliminating E_x, E_z, H_x, and H_z from Eq. (5), we can obtain two coupled-wave equations obeyed by the z-dependent field components $E_y(z)$ and $H_y(z)$. Owing to their continuities at the interface, we introduce a two-component wave function $\phi = \begin{pmatrix} E_y \\ \eta_0 H_y \end{pmatrix}$, which is obviously continuous at the interface, and then we have the wave equation in ϕ,

$$\frac{d}{dz}\left(A^{-1}\frac{d\phi}{dz}\right) - k_0^2 M \phi = 0, \tag{6}$$

with the two z-dependent 2×2 matrices

$$A = \begin{pmatrix} 0 & -1 \\ \varepsilon_3 & 0 \end{pmatrix}, \quad M = \begin{pmatrix} i\frac{\varepsilon_2}{\varepsilon_1}\sin\theta & \frac{\sin^2\theta}{\varepsilon_1} - 1 \\ \varepsilon_1 - \frac{\varepsilon_2^2}{\varepsilon_1} - \sin^2\theta & i\frac{\varepsilon_2}{\varepsilon_1}\sin\theta \end{pmatrix}. \tag{7}$$

Following the invariant imbedding theory generalized by Kim *et al.* [23], we must extend ϕ to a 2×2 matrix, i.e., $\psi = \begin{pmatrix} E_{y1} & E_{y2} \\ \eta_0 H_{y1} & \eta_0 H_{y2} \end{pmatrix}$, where the first column vector stands for the wave function when the incident wave is E_y, i.e., the s-polarized wave, and the second column vector for the wave function when the incident wave is H_y, i.e., the p-polarized wave. We are interested in the 2×2 reflection and transmission coefficient matrices $r(L)$ and $t(L)$, which consist in the wave functions of the incident and transmissive regions, namely,

$$\psi(z) = \begin{cases} e^{-iP(z-L)} + e^{iP(z-L)}r(L), & z \geq L \\ e^{-iPz}t(L), & z \leq 0, \end{cases} \tag{8}$$

where P is a 2×2 diagonal matrix satisfying $P=Ik_0\cos\theta$ and I is the unit matrix. The element $r_{11}(r_{21})$ of r is the reflection coefficient of the $s(p)$-polarized component in the reflected wave when the incident wave is s polarized (i.e., E_y). Likewise, $r_{22}(r_{12})$ is the reflection coefficient of the $p(s)$-polarized component in the reflected wave when the incident wave is p polarized (i.e., H_y). Similar definitions can be applied to the transmission coefficient matrix t [23]. In light of the invariant imbedding theory and after some lengthy algebra, we derive the invariant imbedding equations for $r(\ell)$ and $t(\ell)$ as functions of the so-called imbedding variable ℓ,

$$\frac{dr}{d\ell} = i(rAA_1^{-1}P + AA_1^{-1}Pr) - \frac{i}{2}(I+r)(AA_1^{-1}P + k_0^2P^{-1}A_1M) \times (I+r), \tag{9a}$$

$$\frac{dt}{d\ell} = itAA_1^{-1}P - \frac{i}{2}t(AA_1^{-1}P + k_0^2P^{-1}A_1M)(I+r), \tag{9b}$$

where the matrix $A_1=\left(\begin{smallmatrix}0 & -1\\ 1 & 0\end{smallmatrix}\right)$ is defined by Eq. (7) by setting $\varepsilon_3=1$ for air (the incident medium) and I is the 2×2 unit matrix. With the initial conditions $r(0)=0$ and $t(0)=I$, we can integrate Eqs. (9a) and (9b) numerically from $\ell=0$ to $\ell=L$ and obtain the reflection and transmission coefficient matrices r and t. The field amplitude $\psi(z)$ inside the inhomogeneous plasma can also be calculated by

$$\frac{d\psi(z,l)}{d\ell} = i\psi(z,l)AA_1^{-1}P - \frac{i}{2}\psi(z,l)(AA_1^{-1}P + k_0^2P^{-1}A_1M) \times [I + r(l)], \tag{9c}$$

where ψ is regarded as a function of z and ℓ. For a given $z(0\leq z\leq L)$, $\psi(z,L)$ is obtained by integrating this equation, along with Eq. (9a), from $\ell=z$ to $\ell=L$ with the initial condition $\psi(z,z)=I+r(z,z)$. Then, from Maxwell's equations, we can express the field components E_z and H_z in terms of E_y and H_y,

$$E_z = -\frac{\sin\theta}{\varepsilon_1}\eta_0 H_y - i\frac{\varepsilon_2}{\varepsilon_1}E_y, \quad \eta_0 H_z = E_y\sin\theta. \tag{10}$$

Bearing r and t obtained just in mind, we then discuss the GH shifts in terms of the stationary-phase approach. Let $r_{jm}=|r_{jm}|\exp(i\varphi_{jm})=a_{jm}+ib_{jm}$, where j, $m=1$, 2, a_{jm} and b_{jm} are the real and imaginary parts of r_{jm}, respectively, and φ_{jm} is the phase of r_{jm}. For a given frequency ω (or wavelength λ), the GH shifts Δ_{jm} of the reflected wave for the different polarized components can be determined by [28]

$$\Delta_{jm} = -\frac{\partial\varphi_{jm}}{\partial q} = \frac{\lambda}{2\pi\cos\theta}\frac{b_{jm}a'_{jm} - a_{jm}b'_{jm}}{R_{jm}}, \tag{11}$$

where $R_{jm}=|r_{jm}|^2$ is the reflectivity and $a'_{jm}(b'_{jm})=\frac{\partial a_{jm}(b_{jm})}{\partial\theta}$. Yet, it is worthwhile to notice that Δ_{jm} depends not only on θ, but also on other variables such as ω_c (or the external static magnetic field) and the slab's thickness. Δ_{jm} have the definitions similar to r_{jm}, that is, $\Delta_{11}(\Delta_{21})$ is the GH shift of the $s(p)$-polarized component in the reflected wave when the incident wave is s polarized. Similarly, $\Delta_{22}(\Delta_{12})$ is the GH shift of the $p(s)$-polarized component in the reflected wave when the incident wave is p polarized. Δ_{11} and Δ_{22} are called the copolarized GH shifts, whereas Δ_{12} and Δ_{21} are the cross-polarized ones. Because $r_{12}=-r_{21}$, we have from Eq. (11) $\Delta_{12}=\Delta_{21}$ at any angles of incidence. Moreover, we should stress here that since the s- and p-polarized components of the reflected wave suffer different GH shifts, they become two separate reflected waves, which is dissimilar to the result usually predicted by geometrical optics.

III. NUMERICAL RESULTS AND DISCUSSION

In our calculations, we choose the operating frequency at the local plasma frequency, i.e., $\omega=\omega_0$, and the collision frequency $\nu=10^{-8}\omega_0$. To examine the effects of the medium's inhomogeneity on the GH shifts, below we consider two types of electron-density profiles.

A. Linear electron-density profile

In this case, we assume that $f(z)$ is of the form

$$f(z) = \frac{1}{2}\left(\frac{z}{L}+1\right), \quad 0\leq z\leq L, \tag{12}$$

the curve of which versus z is shown in the upper-left inset of Fig. 1. Before starting our discussion, let us elucidate first the definition of a Brewster angle in a complicated medium such as an anisotropic medium, chiral medium, and magnetized plasma. According to Refs. [29,30], a Brewster angle can be defined as the angle of incidence that makes the copolarized reflectivity null (i.e., $R_{jj}=0$, $j=1$, 2) when a monochromatic plane wave of arbitrary polarization is incident. This means that when an arbitrarily polarized monochromatic plane wave is incident at a Brewster angle, the reflected wave either does not occur or becomes a linearly polarized wave. However, when the copolarized reflectivity never reaches zero in, e.g., an absorbing medium, we can only define the pseudo-Brewster angle at which the copolarized reflectivity attains its minimum (the dip of reflectivity).

Figure 2 displays the dependences of the GH shifts and reflectivity on the angle of incidence for $L=2\lambda$ and $\omega_c=0.3\omega_0$. It is evident from Fig. 2(a) that when the incident wave is s polarized, the copolarized reflectivity R_{11} approaches its minimum (very close to zero) at $\theta=35.1°$, that is, the pseudo-Brewster angle, where the corresponding GH shift Δ_{11} arrives at the negative maximum (about -16λ). This is because when a plane wave is incident at a pseudo-Brewster angle (or Brewster angle), the reflected wave undergoes an abrupt change of phase with respect to the incident wave [31]. The GH shift Δ_{21}, which corresponds to the cross-polarized reflectivity R_{21}, attains its local positive maximum at the pseudo-Brewster angle [see the arrow "1" in Fig. 2(b)]. This indicates that the lateral separation between the s- and p-polarized components of the reflected wave is $0.66\lambda-(-16\lambda)$ when an s-polarized wave is incident at the pseudo-Brewster angle. In addition, we can see from the ar-

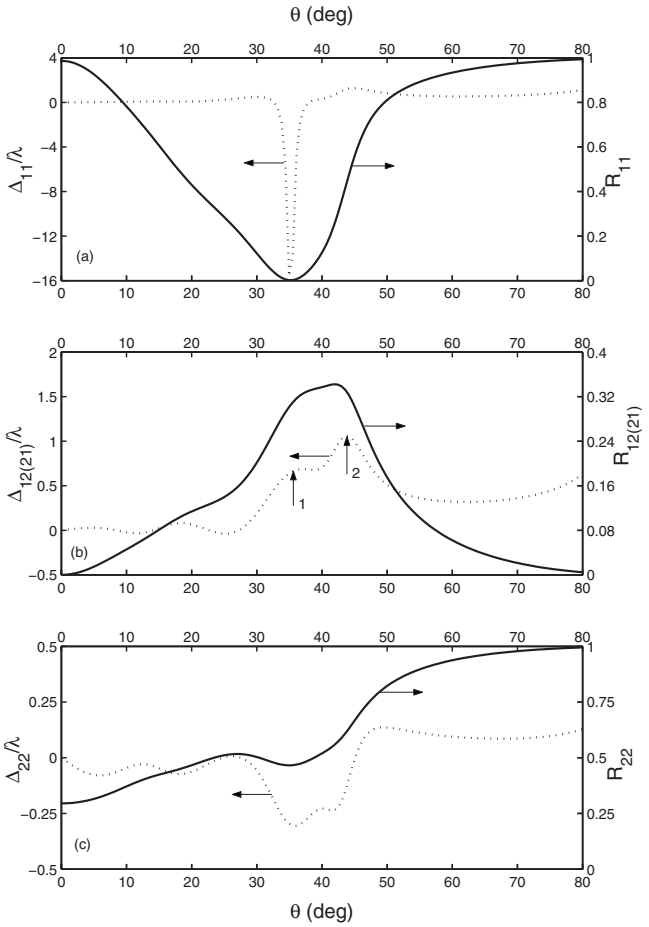

FIG. 2. Dependences of the GH shifts and reflectivity on the angle of incidence for $L=2\lambda$ and $\omega_c=0.3\omega_0$ in the case of the linear electron-density profile. Dotted and solid lines correspond to the GH shifts and reflectivity, respectively. (a) and (c) for the copolarized GH shifts and reflectivity and (b) for the cross-polarized GH shifts and reflectivity.

row "2" in the Fig. 2(b) that Δ_{21} reaches a positive maximum at $\theta=43.9°$, which is in the vicinity of the maximum of R_{21}. When the incident wave is p polarized, the pseudo-Brewster angle is identical to that for the s-polarized incident wave [see Fig. 2(c)]. As expected, Δ_{22} approaches the negative maximum at this angle, albeit very small. At the pseudo-Brewster angle, both the copolarized GH shifts (Δ_{11} and Δ_{22}) are negative, while the cross-polarized GH shifts $\Delta_{12(21)}$ are positive. It is also clear from Figs. 2(a)–2(c) that although the total internal reflection takes place near $\theta=75°$ for both the s- and p-polarized incident waves, no large GH shifts exhibit, as is distinct from isotropic homogenous media.

As for the negative GH shifts occurring here, it can be understood in the following. Usually, a negative GH shift can occur easily in a negatively refractive material; however, in fact, it can also appear under other circumstances, such as absorbing media [28,31], a metallic quantum well [11], and a plasma [32]. It was reported that the backward wave may be supported by a multilayered structure that contains at least one layer with a negative permittivity [6]. The inhomogeneous stratified plasma may be treated as a multilayer which consists of a large number of layers with continuously varying permittivity. We can find readily from Eqs. (4) and (12) that when $z/L>0.82$, $\mathrm{Re}(\varepsilon_1)<0$, while $\mathrm{Re}(\varepsilon_2)>0$ and $\mathrm{Re}(\varepsilon_3)>0$. This implies that our structure can support a backward wave and thus it is possible for a negative GH shift to occur in the structure. Noticeably, the field component E_z is resonantly enhanced at $z/L=0.82$ due to $\mathrm{Re}(\varepsilon_1)=0$ [see Eq. (10)], which might cause intriguing physical effects. To shed further light on the negative GH shift, taking Δ_{11} in Fig. 2(a) as an example, we plot in Fig. 3 the variation of the lateral component $\langle S_x(z)\rangle$ of the time-averaged Poynting vector with the coordinate z for $\theta=35.1°$. Indeed, at $z/\lambda=1.64$ (corresponding to $z/L=0.82$) occurs a giant negative-energy flow, which should exactly lead to the large negative GH shift (-16λ). The insets (a) and (b) of Fig. 3 show the distributions of energy flow $\langle S_x(z)\rangle$ on both the sides of $z/\lambda=1.64$. Obviously, $\langle S_x(z)\rangle$ flows nearly inversely on both the sides. Additionally, the power flow inside the plasma slab is worked out as $\eta_0 P=-835.1$ in terms of $P=(1/2)\int_0^L\langle S_x(z)\rangle dz$.

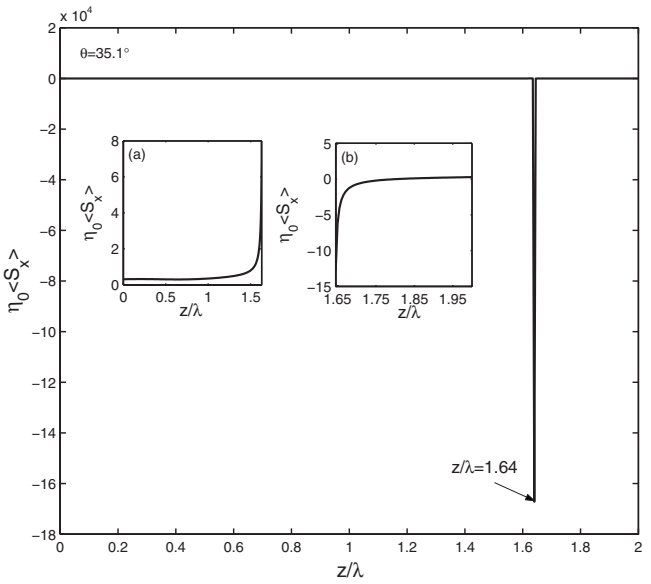

FIG. 3. Variation of the lateral component of the time-averaged Poynting vector $\eta_0\langle S_x(z)\rangle$ inside the plasma slab with the coordinate z for $\theta=35.1°$ and $L=2\lambda$. A giant negative-energy flow occurs at $z/\lambda=1.64$ (corresponding to $z/L=0.82$). Insets (a) and (b) show the distributions of $\eta_0\langle S_x(z)\rangle$ on both the sides of $z/\lambda=1.64$.

The external static magnetic field imposes an influence on the plasma's permittivity through the electron cyclotron frequency ω_c and thus on GH shifts. For the case $\omega_c<\omega_0$, in the calculation, we find that the weaker external magnetic field hardly affects the GH shifts. Therefore, in what follows, we only focus on these ω_c (or external magnetic fields) that strikingly affect the GH shifts. Figure 4 illustrates the variations of the GH shifts with ω_c for $L=2\lambda$ and $\theta=35.1°$, 43.9°, and 75°, which are the angles involved above. We can see from Fig. 4(a) that for $\theta=35.1°$, the GH shift Δ_{11} reaches the negative maximum at $\omega_c/\omega_0=0.3$, which concurs exactly with the result in Fig. 2(a); for $\theta=43.9°$, the shift comes to the negative maximum at $\omega_c/\omega_0=0.380$. It is evident from Figs. 4(a)–4(c) that for $\theta=75°$, the shifts saliently fluctuate between the positive and negative values as the external

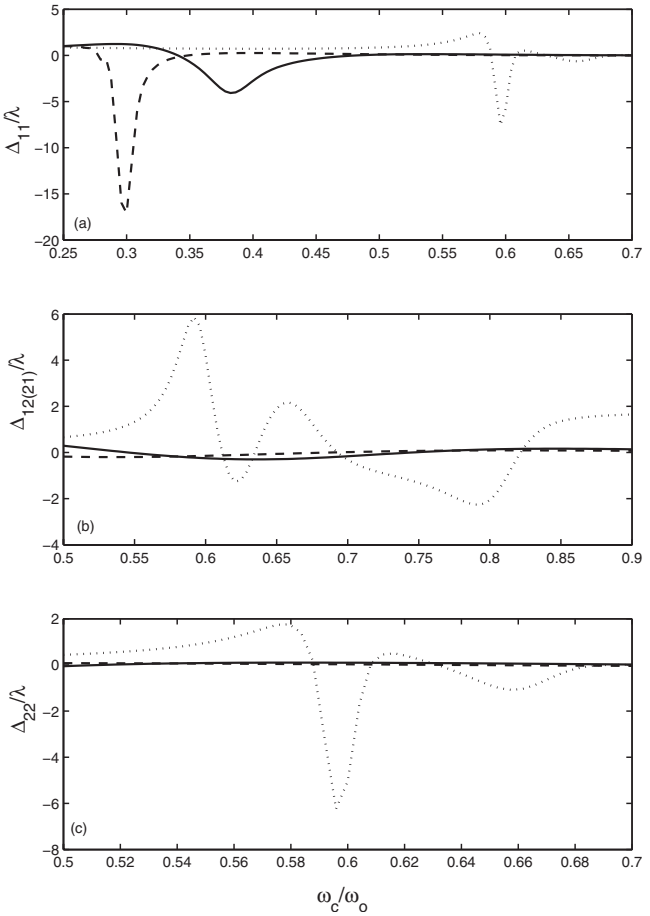

FIG. 4. Variations of the GH shifts with ω_c for $L=2\lambda$ and $\theta=35.1°$, 43.9°, and 75°. The electron-density profile is the same as in Fig. 2. Dashed, solid, and dotted lines correspond to the GH shifts for $\theta=35.1°$, 43.9°, and 75°, respectively. (a) and (c) for the copolarized GH shifts and (b) for the cross-polarized GH shifts.

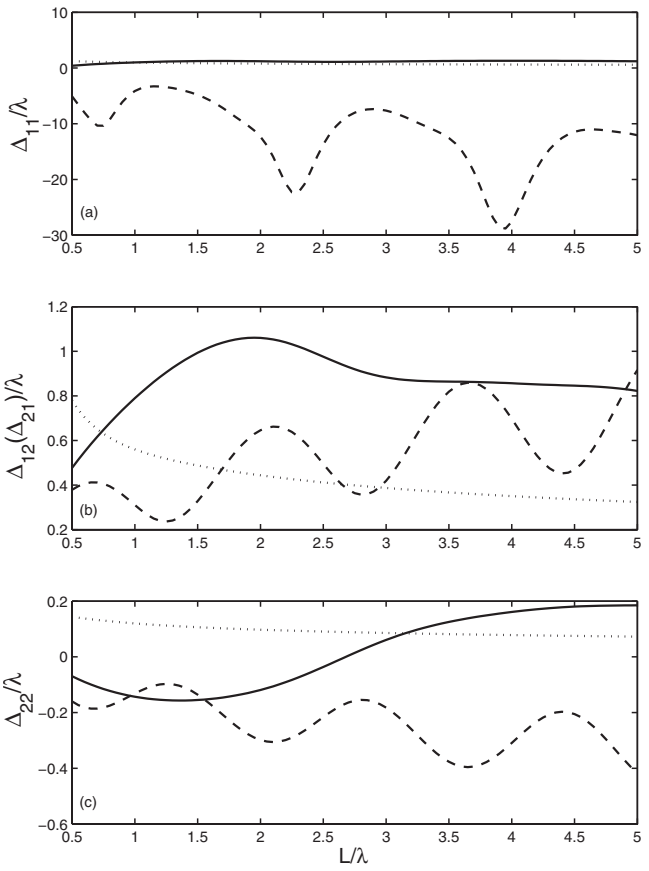

FIG. 5. Variations of the GH shifts with L for $\omega_c=0.3\omega_0$ and $\theta=35.1°$, 43.9°, and 75°. The electron-density profile is the same as in Fig. 2. Dashed, solid, and dotted lines correspond to the GH shifts for $\theta=35.1°$, 43.9°, and 75°, respectively. (a) and (c) for the copolarized GH shifts and (b) for the cross-polarized GH shifts.

magnetic field increases. The changes of the GH shift $\Delta_{12(21)}$ are particularly observable, with its positive and negative maxima at $\omega_c/\omega_0=0.592$ and 0.797, respectively. As a result, for such an angle of incidence, we can switch the GH shifts between the positive and negative values by adjusting the external magnetic field. In contrast, for $\theta=35.1°$ and 43.9°, the stronger external magnetic field $(\omega_c/\omega_0>0.45)$ has hardly effects on the GH shifts, from which we can conjecture that when the angles of incidence are smaller, the stronger external magnetic field exerts practically no influences on the GH shifts.

Next, we discuss briefly the effects of the thickness of the plasma slab on the GH shifts. Figure 5 shows the variations of the GH shifts with L for $\omega_c=0.3\omega_0$ and $\theta=35.1°$, 43.9°, and 75°. It can be seen from the figure that for $\theta=35.1°$, the GH shifts Δ_{11}, $\Delta_{12(21)}$, and Δ_{22} all exhibit the near-periodical oscillation with the slab's thickness and both the copolarized GH shifts are negative and the cross-polarized GH shift is positive. In particular, it should be noted that Δ_{11} becomes considerably large and negative for $\theta=35.1°$, while for $\theta=43.9°$ and 75°, the slab's thickness has a tiny impact on the GH shifts. These results might be interpreted as follows [5,12,33]. A slab structure is often analogous to a Fabry-Perot optical interferometer, where the two interfaces of the slab behave like the partially transparent mirrors. Therefore, the GH shift $\Delta_{11}(\Delta_{22})$ is composed of two parts: one comes from the interference between two reflected waves from the two interfaces of the plasma slab and the other arises from the interference of the reflected wave at the first interface with the incident wave. The former contains a periodical factor with respect to the slab's thickness L and hence the interference leads to the near-periodical oscillation of the GH shift with L; the latter is proportional to L so that when L satisfies the constructive interference condition, the GH shift is suppressed and vice versa. The former dominates the GH shift when the angle of incidence is smaller, otherwise the latter is dominant. Since in this case the former is dominant for $\theta=35.1°$, the near-periodical oscillation of the GH shift with L occurs. However, due to the polarization conversion, the incident TE (TM) wave will not interfere with the reflected TM (TE) wave and then the cross-polarized GH shift $\Delta_{12(21)}$ can only originate from the interference among multiply reflected waves from the two boundaries. Therefore, the near-periodical oscillation of $\Delta_{12(21)}$ with L is kept; meanwhile, this seems to be why $\Delta_{12(21)}$ becomes larger for the higher reflectivity $R_{12(21)}$, as can be seen from the arrows 1 and 2 in Fig. 2(b).

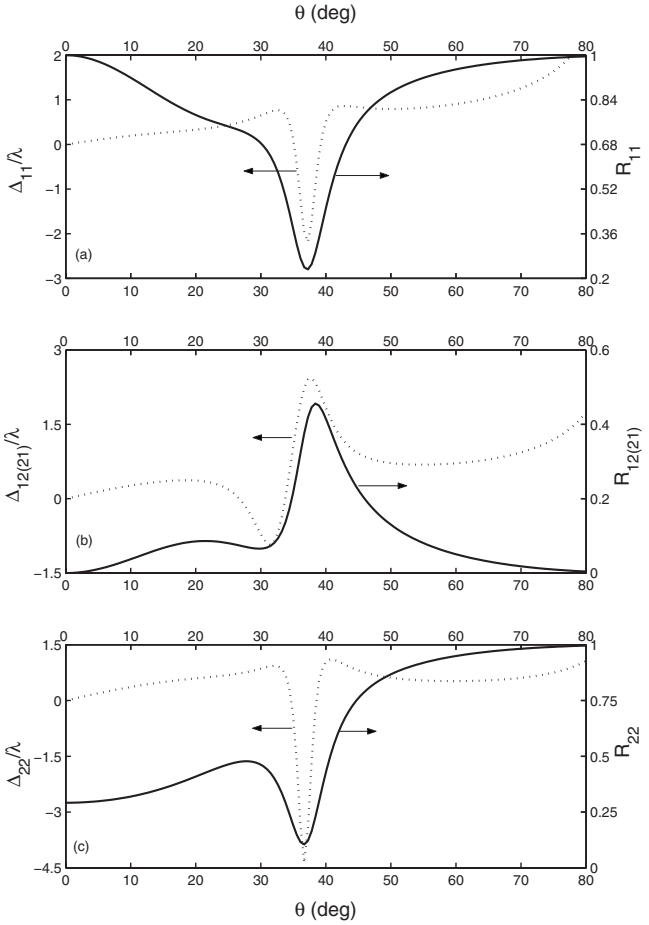

FIG. 6. Dependences of the GH shifts and reflectivity on the angle of incidence for the same parameters as in Fig. 2, but for the parabolic electron-density profile. Dotted and solid lines correspond to the GH shifts and reflectivity, respectively. (a) and (c) for the copolarized GH shifts and reflectivity and (b) for the cross-polarized GH shifts and reflectivity.

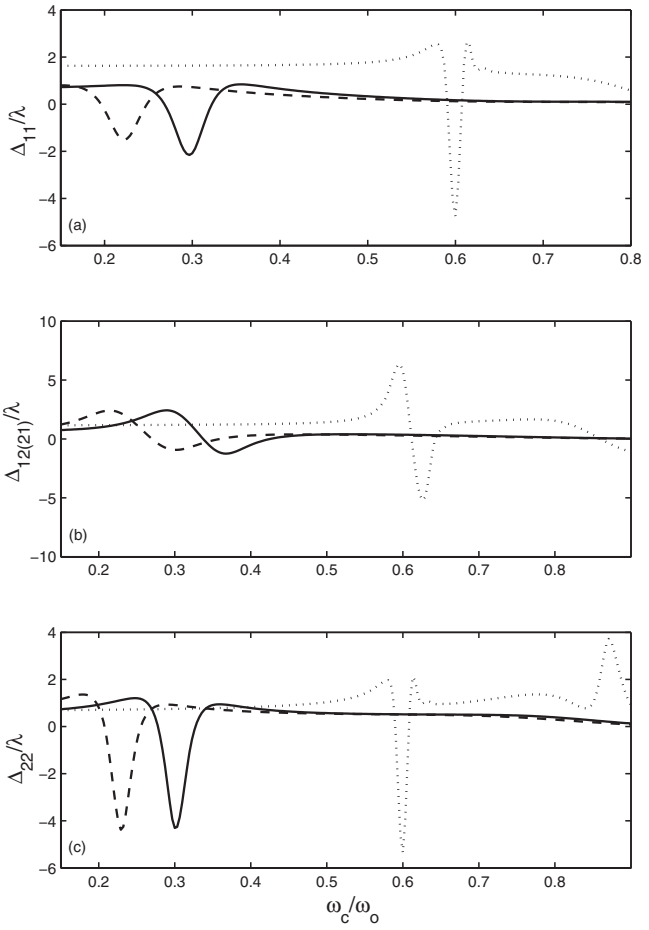

FIG. 7. Dependences of the GH shifts on ω_c for $L=2\lambda$ and $\theta=31.3°$, 37.1°, and 75°. The electron-density profile is the same as in Fig. 6. Dashed, solid, and dotted lines correspond to the GH shifts for $\theta=31.3°$, 37.1°, and 75°, respectively. (a) and (c) for the copolarized GH shifts and (b) for the cross-polarized GH shifts.

B. Parabolic electron-density profile

In this case, let $f(z)$ have the form

$$f(z) = 1 - 2\left(\frac{z}{L} - \frac{1}{2}\right)^2, \quad 0 \le z \le L, \tag{13}$$

the plot of which versus z is shown in the upper-left inset of Fig. 1. Here, $f(z)$ is chosen such that it has the same maximum and minimum as the linear density profile. We depict in Fig. 6 the dependences of the GH shifts and reflectivity on the angle of incidence for the same parameters as in Fig. 2. We can see from Figs. 6(a)–6(c) that the copolarized GH shifts Δ_{11} and Δ_{22} vary similarly and whether the incident wave is s or p polarized, there is a pseudo-Brewster angle at $\theta=37.1°$, where both negative maxima of Δ_{11} and Δ_{22} occur exactly. We can also see from Fig. 6(b) that a peak and dip of the cross-polarized GH shifts $\Delta_{12(21)}$ are located near the pseudo-Brewster angle and at $\theta=31.3°$, respectively. This result can be understood from the corresponding peak and dip of the reflectivity. In addition, no remarkable differences in the magnitude among Δ_{11}, $\Delta_{12(21)}$, and Δ_{22} can be observed, which is different from the linear density profile.

Figure 7 shows the dependences of the GH shifts on ω_c for $L=2\lambda$ and $\theta=31.3°$, 37.1°, and 75°. Clearly, the stronger external magnetic field ($\omega_c/\omega_0>0.45$) exerts practically no influences on the GH shifts for a smaller angle of incidence, as is the same as the linear electron-density profiles. More interestingly, the external magnetic field affects both the copolarized GH shifts in a similar manner, except for a positive maximum near $\omega_c/\omega_0=0.872$ for Δ_{22}. Apparently, Δ_{11} and Δ_{22} for $\theta=31.3°$, 37.1°, and 75° reach the negative maxima near $\omega_c/\omega_0=0.230$, 0.30, and 0.60, respectively, as indicated in Figs. 7(a)–7(c). For the three angles of incidence, the cross-polarized GH shifts vary in a similar scheme with the external magnetic field, *viz.*, the positive and negative GH shifts with nearly equal magnitude can be achieved when ω_c changes in a narrower range, as seen in Fig. 7(b).

The dependences of the GH shifts on the slab's thickness L for $\omega_c=0.3\omega_0$, and $\theta=31.3°$, 37.1°, and 75° are indicated in Fig. 8. Unlike the linear electron-density profile, the variations of the GH shifts with L do not manifest oscillations, which might be due to the fact that the nonlinear density profile destroys the periodicity of the GH shift with respect to L. It is distinct that although the GH shifts Δ_{11} and $\Delta_{12(21)}$

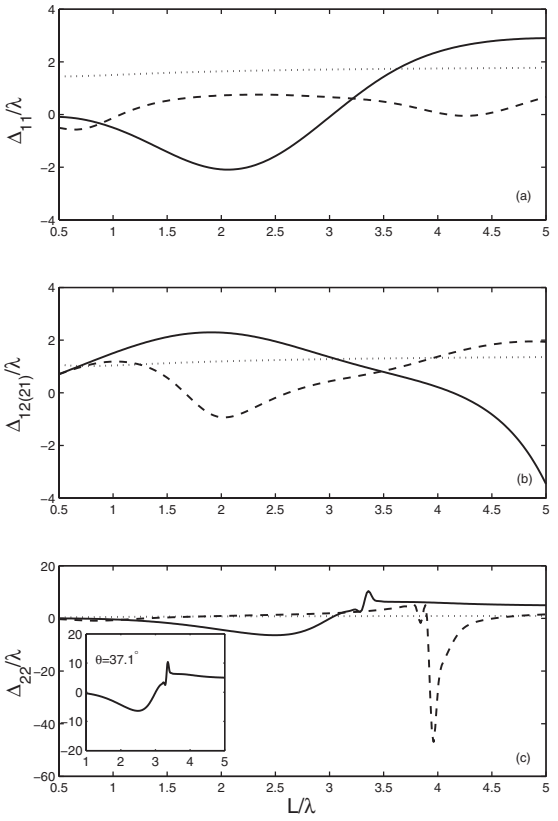

FIG. 8. Dependences of the GH shifts on L for $\omega_c=0.3\omega_0$ and $\theta=31.3°$, 37.1°, and 75°. The electron-density profile is the same as in Fig. 6. Dashed, solid, and dotted lines correspond to the GH shifts for $\theta=31.3°$, 37.1°, and 75°, respectively. (a) and (c) for the copolarized GH shifts and (b) for the cross-polarized GH shifts. The magnified inset in (c) is the GH shifts for $\theta=37.1°$.

exist for $\theta=75°$, they are very small and nearly unchanged with the slab's thickness; for $\theta=31.3°$, 37.1°, the positive or negative GH shifts are always available by adjusting the slab's thickness. It is especially noticeable that the giant negative GH shift $\Delta_{22}(=-46.76\lambda)$ occurs at $L=3.96\lambda$ for $\theta=31.3°$. Actually, the rather considerable positive and negative Δ_{22} are also attainable for $\theta=37.1°$ on altering the slab's thickness, as can be seen in the magnified inset of Fig. 8(c).

IV. CONCLUSIONS

In conclusion, by use of the invariant imbedding theory, we have discussed theoretically the GH shifts of the reflected waves from a cold, inhomogeneous, and magnetized plasma slab. Bearing on the linear and parabolic electron-density profiles, we have demonstrated numerically the dependences of the co- and cross-polarized GH shifts on the angle of incidence, external static magnetic field, and thickness of the plasma slab. The results suggest that when the wave is incident at a pseudo-Brewster, the copolarized GH shifts can attain their negative maxima, which arises from the abrupt change of phases suffered by the reflected waves. The GH shifts can be switched between the positive and negative values at certain angles of incidence by adjusting the external magnetic field; particularly, the large and negative GH shifts are obtained for some external magnetic fields. The different electron-density profiles of plasma can give rise to the very different dependences of the GH shifts on the angle of incidence, external magnetic field, and the slab's thickness. By way of example, we also provide an explanation for the giant negative GH shift Δ_{11} in the linear electron-density profile case. Of particular interest is that without changing the structure of the plasma slab, the GH shifts can be manipulated by modifying the angle of incident or the external magnetic field.

ACKNOWLEDGMENTS

The authors would like to express their gratitude to the referees, whose searching questions and suggestions helped them elaborate and improve the paper. They also wish to thank Dr. J. Sun for helpful discussions.

[1] F. Goos and H. Hänchen, Ann. Phys. **436**, 333 (1947).
[2] F. Goos and H. Hänchen, Ann. Phys. **440**, 251 (1949).
[3] K. Artmann, Ann. Phys. **2**, 87 (1949).
[4] K. V. Lotsch, Optik **32**, 116 (1970); **32**, 189 (1970); **32**, 299 (1971); **32**, 553 (1971).
[5] C.-F. Li, Phys. Rev. Lett. **91**, 133903 (2003).
[6] T. Tamir and H. L. Bertoni, J. Opt. Soc. Am. **61**, 1397 (1971).
[7] V. Shah and T. Tamir, J. Opt. Soc. Am. **73**, 37 (1983).
[8] L. A. A. Read, M. Wong, and G. E. Reesor, J. Opt. Soc. Am. **68**, 319 (1978).
[9] R. P. Riesz and R. Simon, J. Opt. Soc. Am. A **2**, 1809 (1985).
[10] C. W. Hsue and T. Tamir, J. Opt. Soc. Am. A **2**, 978 (1985).
[11] J. Broe and O. Keller, J. Opt. Soc. Am. A Opt. Image Sci. Vis. **19**, 1212 (2002).
[12] X. Chen and C.-F. Li, Phys. Rev. E **69**, 066617 (2004).
[13] I. V. Shadrivov, A. A. Zharov, and Y. S. Kivshar, Appl. Phys. Lett. **83**, 2713 (2003).
[14] N. H. Shen, J. Chen, Q. Y. Wu, T. Lan, Y. X. Fan, and H. T. Wang, Opt. Express **14**, 10574 (2006).
[15] Y. Xiang, X. Dai, and S. Wen, Appl. Phys. A: Mater. Sci. Process. **87**, 285 (2007).
[16] X. Chen, M. Shen, Z. F. Zhang, and C.-F. Li, J. Appl. Phys. **104**, 123101 (2008).
[17] H. Huang, Y. Fan, B.-I. Wu, and J. A. Kong, Appl. Phys. A: Mater. Sci. Process. **94**, 917 (2009).
[18] L.-G. Wang, M. Ikram, and M. S. Zubairy, Phys. Rev. A **77**, 023811 (2008).
[19] D. Felbacq, A. Moreau, and R. Smaâli, Opt. Lett. **28**, 1633 (2003).
[20] L.-G. Wang and S.-Y. Zhu, Opt. Lett. **31**, 101 (2006).
[21] P. Mazur and B. Djafari-Rouhani, Phys. Rev. B **30**, 6759 (1984).
[22] H. Zhou, X. Chen, P. Hou, and C.-F. Li, Opt. Lett. **33**, 1249 (2008).

[23] K. Kim, D.-H. Lee, and H. Lim, Europhys. Lett. **69**, 207 (2005).
[24] K. Kim and D.-H. Lee, Phys. Plasmas **12**, 062101 (2005).
[25] K. Kim and D.-H. Lee, Phys. Plasmas **13**, 042103 (2006).
[26] K. Kim, D. K. Phung, F. Rotermund, and H. Lim, Opt. Express **16**, 15506 (2008).
[27] K. Kim, Phys. Rev. B **58**, 6153 (1998).
[28] L.-G. Wang, H. Chen, and S.-Y. Zhu, Opt. Lett. **30**, 2936 (2005).
[29] S. Bassiri, C. H. Papas, and N. Engheta, J. Opt. Soc. Am. A **5**, 1450 (1988).
[30] J. Lekner, Pure Appl. Opt. **5**, 417 (1996).
[31] H. M. Lai and S. W. Chan, Opt. Lett. **27**, 680 (2002).
[32] T. Tamir and A. A. Oliner, Proc. IEEE **51**, 317 (1963).
[33] L.-G. Wang, H. Chen, N.-H. Liu, and S.-Y. Zhu, Opt. Lett. **31**, 1124 (2006).